SARS-CoV-2-induced impaired immune response by Prostaglandin E2 is accelerated by age, male sex and air pollution

Melanie Ricke-Hoch
Hannover Medical School
Elisabeth Stelling
Hannover Medical School
Lisa Lasswitz
TWINCORE, Center for Experimental and Clinical Infection Research Hannover
Antonia-Patricia Gunesch
TWINCORE, Center for Experimental and Clinical Infection Research Hannover
Martina Kasten
Hannover Medical School
Francisco J. Zapatero-Belinchón
TWINCORE, Center for Experimental and Clinical Infection Research Hannover
Graham Brogden
TWINCORE, Center for Experimental and Clinical Infection Research Hannover
Gisa Gerold
TWINCORE, Center for Experimental and Clinical Infection Research Hannover
Karin Battmer
Hannover Medical School
Thomas Pietschmann
Division of Experimental Virology, TWINCORE
Virginie Montiel
Université catholique de Louvain (UCLouvain)
Jean-Luc Balligand
Université catholique de Louvain, Institut de Recherche Expérimentale et Clinique
Federica Facciotti
Department of Experimental Oncology, IEO European Institute of Oncology IRCCS
https://orcid.org/0000-0002-2541-9428
Emilio Hirsch
University of Torino, Italy https://orcid.org/0000-0002-9073-6024
Husni Elbahesh
University of Veterinary Medicine

Guus Rimmelzwaan
University of Veterinary Medicine
Anne Hoefer
Hannover Medical School
Mark Kühnel
Institute for Pathology, Hannover Medical School, Hannover,
Danny Jonigk
Hannover Medical School
Julian Eigendorf
Hannover Medical School
Uwe Tegtbur
Hannover Medical School
Lena Mink
Hannover Medical School
Michaela Scherr
Hannover Medical School
Thomas Illig
Institute of Epidemiology, Helmholtz Center Munich
Axel Schambach
Hannover Medical School
Tobias Pfeffer
Hannover Medical School
Birgit Andrée
Hannover Medical School
Andres Hilfiker
Hannover Medical School
Axel Haverich
Medical School Hannover
Denise Hilfiker-Kleiner (Hilfiker.Denise@mh-hannover.de)
Hannover Medical School

Article

Keywords: SARS-CoV-2, COVID-19, Prostaglandin E2, immune response

Posted Date: December 31st, 2020

DOI: https://doi.org/10.21203/rs.3.rs-129664/v1

Abstract

The SARS-CoV-2 coronavirus has led to a pandemic with millions of people affected. The present study finds prostaglandin E2 (PGE2) blood levels elevated in COVID-19 patients with positive correlation with disease severity. SARS-CoV-2 induces PGE2 generation and secretion in infected lung epithelial cells by upregulating cyclo-oxygenase (COX)-2 and reducing the PG-degrading enzyme 15-hydroxyprostaglandin-dehydrogenase. Also living human-lung-precision-slices infected with SARS-CoV-2 display upregulated COX-2. PGE2 in serum of COVID-19 patients lowers the expression of Paired-Box-Protein-Pax-5 (PAX5), a master regulator of B-cell survival, proliferation and differentiation, in both human and mouse pre-B-cells, while the PGE2 inhibitor taxifolin directly reduces SARS-CoV-2-induced PGE2 production and attenuates viral replication. Risk-factors for severe disease courses, i.e. older age, male sex and air pollution are associated with higher PGE2 production and lower PAX5 expression in pre-B-cells. Since PGE2 acts broadly immunosuppressive its elevation might reduce the early anti-viral defense and its inhibition may therefore reduce severe disease courses.

Introduction

The 2019 strain of coronavirus (severe acute respiratory syndrome coronavirus-2 SARS-CoV-2) caused a pandemic with COVID-19 disease affecting millions of people worldwide. Many infected patients remain asymptomatic or develop only mild symptoms, but they are nonetheless fully capable of transmitting the virus [1, 2]. Patients with more serious disease courses frequently present with severe acute respiratory syndrome that can progress to pneumonia and acute respiratory distress syndrome and shock [1, 2, 3]. Systemic inflammation, acute cardiac injury, heart failure, and hypercoagulability are critical complications in COVID-19 disease [3, 4, 5, 6, 7, 8, 9]. Cell types infected with SARS-CoV-2 include pulmonary epithelial cells, renal cells, cardiomyocytes, endothelial cells and pericytes have been identified [10, 11, 12].

An increased risk for infection and severe disease courses have been found in association with older age, male sex, cardiovascular comorbidities and air pollution [7, 13, 14, 15]. Immunothrombosis integrates innate immunity, activation of platelets, and clotting factors to fight invading pathogens and concurrently promotes inflammation-related tissue damage; in the context of COVID-19 disease, this may explain the systemic hypercoagulability frequently present in COVID-19 patients [8]. Further alterations in the immune system with in part opposing mechanisms have been reported in acute and chronic COVID-19 disease. On one hand, COVID-19 infection appears associated with an upregulation and activation of neutrophils while at the same time lymphocytes are diminished [16]. Reduced lymphocyte populations seem to correlate with more severe organ injury and higher mortality in hospitalized COVID-19 patients [16]. In this regard, T-cell exhaustion [2, 17], reduced circulating and resident B-cell population and loss of germinal centers that correlate with viral persistence and severe disease courses correlate with high mortality in the acute phase [2, 18, 19]. In turn, a growing body of clinical data suggests that a cytokine storm is associated with COVID-19 severity and is also a crucial cause of death from COVID-19 [20, 21, 22]. Among potential mechanisms, SARS-CoV-2 induced formation of autoantibodies, tissue and organ injury as well

as secondary infection with bacteria and fungi may be responsible for overshooting inflammation in COVID-19 patients [23] [24].

Prostaglandin (PG) E2, a metabolite of arachidonic acid, is a well-known modulator of viral infection [25]. As such, PGE2 suppresses the adaptive and innate immune systems and promotes infection, e.g., by influenza A virus (IAV) [26, 27]. Moreover, increased circulating PGE2 levels have been associated with reduced immunity in response to IAV vaccination [26, 27]. Interestingly, IAV infection also promotes the production of PGE2 [28]. Cyclooxygenase-2 (COX-2) is a rate-limiting enzyme for the generation of PGE2 and Hydroxyprostaglandin Dehydrogenase 15-(NAD) (HPGD) is an enzyme responsible for the degradation of PGE2 [29]. These findings, supported further by a recent literature review [30] naturally suggested a connection between arachidonic acid metabolism and PGE2 in COVID-19 disease.

We hypothesized that PGE2 modulates the immune response in individuals at risk for severe COVID-19 disease. To test this, we first measured serum PGE2 levels in COVID-19 patients with different levels of disease severity, as well as in subjects with putative risk factors (age, sex, physical fitness, exposure to air pollution) for a severe disease course. To analyzed the direct effects of SARS-CoV-2 on PGE2 production, we infected human lung epithelial cells and human precision-cut-lung-slices (PCLS) with SARS-CoV-2. Additionally, we further dissected the mechanisms of PGE2 modulation of immune defense, e.g. through B-cell maturation and the formation of memory cells, and correlated disease severity with lung B-cell content in patient samples. We further tested strategies to reduce PGE2 production or effect on the above parameters as preventive or therapeutic modalities against severe COVID-19.

Results

Circulating levels of PGE2 in COVID-19 patients and sex- and age-matched healthy controls

We analyzed PGE2 levels in individuals with mild/moderate (n=41) and severe (n=48) COVID-19 disease from hospitals in Hanover (Germany), Milan (Italy) and Brussels (Belgium) and age- and sex-matched healthy controls (n=29) (Table 1, S3). Clinical data and laboratory characteristics of the COVID-19 patients revealed that the more severely affected patients were significantly older with a higher proportion of males than females compared with the mildly/moderately affected group (Table 1). BMI and diabetes rate are increased in the entire COVID-19 cohort with no significant difference between the mild/moderate and the severe groups (Table 1). In addition, C reactive protein (CRP) was elevated, while the total leukocyte- and neutrophil counts were within the normal range, although some patients displayed markedly increased levels (Table 1). The mean lymphocyte counts (T- and B-cells) were reduced in the majority of COVID-19 patients and were specifically low in patients with severe disease courses (Table 1). Platelets were in the normal range in all COVID-19 patient groups and lactate dehydrogenase (LDH) was increased and highest in the severely affected patients (Table 1). Mortality was 15% for the entire cohort with no patient deaths in the mild/moderate group and 27% of patients dying in the severe disease group (Table 1). Circulating PGE2 levels were increased in COVID-19 patients at the time of hospitalization

compared with healthy controls, and PGE2 levels were significantly higher in the severely affected patients compared with the mild/moderate COVID-19 patients (Fig. 1A, B, Table 1).

Expression of COX-2 and HPGD and secretion of PGE2 in human lung epithelial cells and precision-cut lung slices infected with SARS-CoV-2

Next, we investigated whether SARS-CoV-2 would enhance PGE2 production in infected host cells. Human lung epithelial cells (Calu-3 cells) were infected with SARS-CoV-2 (strain SARS-CoV-2/München-1.2/2020/984,p3) [31] and infection was confirmed with qRT-PCR for the SARS-CoV-2 gene encoding nonstructural protein (NSP)7 [32] (Fig. 2A). Infected cells displayed increased secretion of PGE2, which was prevented by incubation with the PGE2 inhibitor taxifolin [33, 34] (Fig. 2B). Taxifolin also slightly but significantly reduced virus production in Calu-3 cells (sFig. 1A). SARS-CoV-2 infection increased the expression of COX-2 and reduced the expression of the PGE2 degrading enzyme HPGD, but did not alter the expression of the PGE synthase (PTGES) in Calu-3 cells (Fig. 2C-E). Also, the *ex vivo* infection of living human PCLS with SARS-CoV-2 (viral infection analyzed by NSP7 qRT-PCR, Fig. 2F) led to an upregulation of COX-2 expression compared with non-infected control slices, while HPGD mRNA levels were unchanged and prostaglandin E synthase (PTGES) expression tended to be increased (Fig. 2G-I).

Effect of PGE2 on the expression of pre-B-cell differentiation and survival factor PAX5 in human pre-B-cells

PGE2 is known to attenuate the proliferation, differentiation and survival of B-cells [35, 36]. Here, we observed that the addition of PGE2 (10 µM, i.e. 3525 pg/ml), in the range measured in COVID-19 patients' sera (1300 to >20.000 pg/ml), to two human B-cell precursor lines, 697 and SUP-B15, significantly reduced PAX5 mRNA expression (Fig. 3A, B). This effect was blocked upon co-treatment with the PGE2 receptor 4 (EP4) antagonist, GW627368 but not with the EP2 receptor antagonist, AH6809 (Fig. 3A).

Effect of serum from COVID-19 patients on PAX5 expression in human pre-B-cells

Serum from COVID-19 patients with elevated PGE2 levels reduced the expression of PAX5 in SUP-B15 cells compared with serum from healthy controls. Again, this effect was blocked upon co-treatment with the PGE2 receptor 4 (EP4) antagonist, GW627368 (Fig. 3C).

Analyses of B-cells in lungs from patients who died of severe acute COVID-19 disease compared with healthy controls and transplant rejection biopsies

In lung biopsies from patients who died of severe acute COVID-19 disease (AC group, confirmed by qRT-PCR for NSP7, Fig. 3D), the signals for CD20 pre-B-cells (qRT-PCR and immunohistochemical quantification) and plasma cells (qRT-PCR for CD138) were barely detectable and lower than in control lung tissue (ctrl) and markedly lower than in lung tissue obtained after transplant rejection (TR, Fig. 3E-H). Lung tissue immunostaining showed increased numbers of $CD68^+$ macrophages and $CD4^+$ T-cells in AC and TR compared with ctrl lung biopsies (Fig. 3E).

Analyses of IL-17A, a marker for pro-inflammatory TH17 cells in lung tissue and in serum from patients with COVID-19 disease

Previous reports suggest that PGE2 upregulates IL-17A and thereby promotes the formation of pro-inflammatory TH17 T-cells [37, 38]. However, IL-17A measured by ELISA was below detection level in the serum from all controls and the majority of COVID-19 patients (sFig. 2A).

ffect of diesel exhaust particles as air pollutants on COX-2 expression and PGE2 secretion in human endothelial cells

To investigate whether air pollution, which has been suggested as an additional risk factor for severe COVID-19 disease [14, 15], affects circulating PGE2 levels, we stimulated primary human cardiac endothelial cells (hCEC) with diesel exhaust particles (DEP). DEP stimulation of hCECs increased PGE2 secretion into the cell culture supernatants of hCECs (Fig. 4A, B). This was associated with the upregulation of COX-2 expression (Fig. 4B). In turn, the DEP-induced PGE2 secretion in hCECs was prevented by treatment with taxifolin [33, 34] (Fig. 4A, B).

PGE2 levels in healthy individuals in relation to sex and age

In healthy control individuals aged <50, circulating PGE2 levels were higher (P>0.01) in men than in women (Fig. 5A). Circulating PGE2 levels were markedly higher in older (>60 years) healthy males and females than in respective sex-matched younger (<50 years) individuals (Fig. 5B). Both males and females showed a significant positive correlation of circulating PGE2 levels with age (Fig. 5D, E), while no correlation with BMI, body weight (BW) or body fat content was observed (Table S4, sFig. 3). Controlled physical exercise for 12 months reduced PGE2 in elderly male and female individuals compared with their baseline (BL) levels (Fig. 5F-G, Table S4). PAX5 expression was higher in 697 and SUP-B15 pre-B-cells incubated with serum from elderly individuals collected after 12 months of controlled physical exercise compared with the BL serum of the same individuals (Fig. 5H, I, Table S4). In addition, the EP4 antagonist, GW627368 increased PAX5 in 697 and SUP-B15 pre-B-cells exposed to BL serum, indicating that the suppressive effect is mediated by PGE2-EP4 (Fig. 5J, K).

Cardiac PGE2 secretion and cardiac PAX5 expression in male mice with impaired androgen receptor signaling in cardiomyocytes

We showed previously that cardiac STAT3 deficiency in mice (STAT3-CKO) leads to the upregulation of COX-2 in both sexes, while HPGD is reduced only in male STAT3-CKO mice due to impaired androgen receptor (AR) signaling [39]. Here, we observed that PGE2 levels secreted from cardiomyocytes of male STAT3-CKO were significantly higher compared with cardiomyocytes from WT mice, while no such differences were observed between female STAT3-CKO and WT-cardiomyocytes (Fig. 6A, B). The treatment of male STAT3-CKO mice with the COX inhibitor ibuprofen (10 mg/kg bodyweight) for two weeks markedly reduced PGE2 secretion in isolated cardiomyocytes (Fig. 6C). Resident Sca-1 positive cardiac progenitor cells (CPC), of which pre-B-cells are a subpopulation (0.38% are Sca-1$^+$/CD19$^+$; Fig. 6D-

G) display lower PAX5 mRNA levels when isolated from STAT3-CKO compared with CPC isolated from WT male hearts; conversely, no difference in PAX5 mRNA levels was observed in CPC from young female STAT3-CKO and WT hearts (Fig. 6H, K). Stimulation of isolated WT-CPC with PGE2 in culture reduced PAX5 expression (Fig. 6L, M, $-7.5x10^3$-fold, $P<0.01$).

Discussion

The key finding of this study is that PGE2 is elevated in patients with COVID-19 disease, with the highest blood levels observed in those severely affected by COVID-19. Since PGE2 exerts immunosuppressive effects on T- and B-cells and monocytes, its elevation might critically reduce the initial anti-viral defense in the early phase of infection and thereby lead to more severe disease courses. Interestingly, our data show that the SARS-CoV-2 virus, not only hijacks the host cell gene expression machinery in order to replicate, but also forces infected host cells to produce PGE2 by upregulating the PGE-generating enzyme COX-2, and at least in part by reducing the expression of the PGE2-degrading enzyme HPGD (Fig. 7). In addition, we provide evidence that reported risk factors for more severe COVID-19 disease courses, i.e. male sex, age and a sedentary life style [13, 40] as well as air pollution [14, 15], are either associated with higher PGE2 levels or directly increase the production of PGE2 (Fig. 7). Our study shows that PGE2 serum levels are higher in men than women. In elderly (>60 years) patients, PGE2 levels are higher than in younger individuals and were reduced by regular exercise. We provide evidence that age-related AR-dysfunction may lead to a higher PGE2 production (Fig. 7) and show that DEP, a component of air pollution, increases the production of PGE2 in endothelial cells, an aspect that has also been reported for airway epithelial cells [41, 42] (Fig. 7). Mechanistically, we demonstrate that PGE2 in serum from COVID-19 patients via its EP4 receptor reduces the expression of PAX5 in human pre-B-cell lines (Fig. 7). PAX5 is a B-cell specific transcription factor responsible for pre-B-cell survival, proliferation, and differentiation [43, 44, 45] and reduced PAX5 therefore reduces the B-cell population, an observation we made in the lung tissue of patients who died of COVID-19 and one that fits well with the recently reported absence of germinal centers and reduction in Bcl-6^+ germinal center B-cells in the lymphatic system of patients who died of COVID-19 [19]. PGE2 impacts not only on B-cells, also targets the innate (monocytes/macrophages) and adaptive (T-cells) immune systems in response to viral infections, evidenced by the lowering of the immune response and the formation of immunity [25, 26, 27]. Based on the hypothesized key role of PGE2 in COVID-19 disease, we provide evidence supporting the benefit of lowering PGE2 levels during SARS-CoV-2 infection either by the use of COX-inhibitors such as ibuprofen or by more specific PGE2 inhibitors such as taxifolin. Furthermore, our data also suggest that regular exercise and reducing air pollution would lower PGE2 levels and, with this, reduce the risk for severe COVID-19 disease (Fig. 7).

PGE2 directly alters B- and T-cells by negatively affecting their proliferation and survival and altering their differentiation [35, 36, 37, 38]. PGE2 suppresses B-cells' continued growth and differentiation and thereby regulates their B-cell responses against pathogens [46], as well as their proliferation and survival [47]. Here, we report that PGE2 reduces the expression of PAX5 in human pre-B-cells via its EP4 receptor. PAX5 is a master regulator of most aspects of the life cycle of B-cells by controlling genes that are required for early

development, antigen-receptor recombination, signaling and adhesion. PAX5 represses the transcription of genes required for the development of other hematopoietic lineages and plasma cells [43, 44, 45]. In fact, the reduction of PAX5 is important for the final differentiation of short-lived plasma cells and their antibody (AB) production. In this regard, a PGE2-mediated reduction of PAX5 not only reduces the number of pre-B-cells, but also boosts the differentiation of B-cells towards plasma cells. This initially leads to high SARS-CoV-2-directed AB titers, but at the price of the depletion of B-cell pools in the long run. Indeed, a severe disease course in patients who died of severe COVID-19 is associated with a reduction in germinal centers [19] and with low $CD20^+$ B-cells counts in lung tissue. Postmortem analyses in patients who died of COVID-19 disease showed no significant lymphocyte invasion in cardiac tissue despite the presence of SARS-CoV-2 particles [10, 11]. Accordingly, a lower percentage and count in $CD3^+$, $CD4^+$, and $CD8^+$ lymphocytes populations have strong predictive values for in-hospital mortality, organ injury, and severe pneumonia [16]. Additional studies suggest higher risks for severe disease courses in COVID-19 patients with dysfunctional B-cells due to common variable immune deficiencies (CVIDs) [18]; correspondingly, patients with larger pools of naïve B-cells seem to build a more effective immune response to SARS-CoV-2 [48].

PAX5 expression is also necessary for the development of memory B-cells after follicular B-cells have encountered antigens [45, 49]. In this regard, elevated PGE2 would also reduce the ability of an organism to develop longstanding immunity after COVID-19 infection. Indeed, there are reports on reinfection in individuals with SARS-CoV-2 [50, 51] including a recent case report of a patient with a $CD20^+$ B-cell acute lymphoblastic leukemia who developed high AB titers against COVID-19 after an initial recovery. However, the patient experienced a viral reactivation after she lost her COVID-19 AB following the administration of rituximab, cytarabine, and dasatinib for her leukemia, and experienced severe COVID-19 pneumonia with lymphopenia and high inflammatory markers [52]. PGE2 not only affects B-cells, but also promotes T-cell exhaustion and viral expansion through EP2 and EP4, as revealed by recent studies [53]. Moreover, immunosuppression caused by T-cell depletion and exhaustion have been suggested as contributing to viral persistence and mortality in COVID-19 patients [2]. PGE2 also impacts on the innate immune system, i.e. monocytes/macrophages, where it exerts anti-inflammatory effects and lowers the release of pro-inflammatory cytokines [54 55].

Using our mouse model of premature age-related heart failure (STAT3-CKO), we also addressed the question of whether PGE2 may be involved in the predisposition of males for severe COVID-19 disease and the frequently observed cardiac complications in COVID-19 patients. In this model, we showed that impaired AR-signaling promotes PGE2 production in the heart of male mice but not in females due to an insufficient expression of HPGD [39]. Of note, impaired AR signaling in humans due to an age-related decrease in circulating testosterone is present in around 20% of men >60 years, 30% of men > 70 years and 50% of men >80 years [56]. The resulting increased PGE2 abundance in our mouse cardiac tissues was associated with a lower expression of PAX5 in cardiac pre-B-cells. The causal role of PGE2 was confirmed via the direct addition of PGE2-reduced PAX5 in WT-CPC *in vitro*. These observations highlight the

influence of local PGE2 production on the heart's immune response and its contribution to the high prevalence of cardiac complications and heart failure in COVID-19 patients [57].

Finally, our study shows for the first time, that PCLS can be used as a disease model to study SARS-CoV-2 infection in human tissues. In addition, it unveils potential therapeutic avenues to reverse the adverse effects on the immune system by reducing PGE2 production. First, we show that the PGE2 inhibitor taxifolin, also known as dihydroquercetin, efficiently reduces SARS-CoV-2-induced PGE2 production in lung cells, e.g. in endothelial cells exposed to DEP (Fig. 7A). Additionally, taxifolin slightly reduced the SARS-CoV-2 virus production in lung cells, an observation supported by a recent publication on screening for natural inhibitors for SARS-CoV-2 *in silico,* which identified taxifolin as a direct inhibitor of the SARS-CoV-2 main protease [58] and suggested that taxifolin may also have antiviral potential (Fig. 7A). Taxifolin is a potent flavonoid with anti-inflammatory activity, which is present as a natural compound in vegetables and fruits and the Siberian larch, *Larix sibirica*, [33, 34]. It is readily available in foodstuffs and could be tested directly in COVID-19 patients. Inhibition of the microsomal prostaglandin E synthase-1 (mPGES-1) by sonlicromanol (Khondrion; a drug currently in phase 2b studies for mitochondrial disease), may also be beneficial in COVID-19 patients (Fig. 7A). Furthermore, using the STAT3-CKO mouse model, we demonstrated that the COX- inhibitor, ibuprofen, reduced PGE2 production in male cardiomyocytes (Fig. 7A). We also provide evidence that enhanced physical activity lowers PGE2 in the elderly and may thereby support their immune systems in fighting SARS-CoV-2 infection (Fig. 7A).

In conclusion, our data suggest that PGE2 plays an important role in severe COVID-19 disease courses, either induced by SARS-CoV-2 or produced by endogenous and exogenous risk factors (Fig. 7A). Mechanistically, we show that PGE2 in COVID-19 disease specifically targets B-cells by reducing PAX5, a key factor for B-cell proliferation and differentiation (Fig. 7A+B). Reducing PGE2 preventively and/or during COVID-19 disease may therefore provide a valuable therapeutic strategy to prevent and fight SARS-CoV-2 infection and to enhance and prolong immunity.

Limitations of the study

Limitations of our study include the limited numbers of blood samples from COVID-19 patients and that clinical data on COVID-19 patients, i.e. as C-reactive protein (CRP), lactate dehydrogenase (LDH), leukocytes normal count, neutrophils normal count, and lymphocytes were not available for all patients.

Materials And Methods

Unless otherwise stated, chemicals and reagents were all purchased from Sigma-Aldrich.

Study design

The aim of the study is to determine the secretion of circulating PGE2 levels in dependence of several risk factors in mild and severe diseased COVID-19 patients compared to healthy individuals, and how PGE2 modulates the host's immune response.

COVID-19 study: In this study of 89 patients diagnosed with COVID-19, 41 presented with mild/moderate symptoms and 48 were hospitalized with severe disease. Blood samples were also obtained from male (n=18) and female subjects (n=28) (age 18-50 years) from a healthy population established by Hannover Unified Biobank (HUB).

The local ethics committees at Hannover Medical School, Comité d'Ethique Hospitalo-Facultaire of UCLouvain, and the Ethical Committee of IEO has been obtained (IEO1271) approved this study. All patients and healthy control subjects provided written informed consent. The study conforms to the principles outlined in the Declaration of Helsinki.

Physical assessment and exercise program in healthy elderly individuals **(**Rebirth 60plus cohort, DRKS00013885) All subjects in the Rebirth 60plus cohort (DRKS00013885) were initially tested for maximum power output on a cycle ergometer with graded exercise test (GXT). Based on their activities, physical fitness and pathologies, each subject was given an aerobic exercise training program. Once a month, the subjects were contacted by phone to assess training progress and adjust the exercise program, if necessary. All subjects of the Rebirth 60plus study were informed about benefits and risks regarding all study procedures. Height and weight were measured using a scale (seca gmbh & co. kg, Hamburg, Germany). Body fat was measured with a medical Body Composition Analyzer mBCA (seca gmbh & co. kg, Hamburg, Germany). The physical activity was tracked using a GPS watch Forerunner 30 (Garmin Deutschland GmbH, Munich, Germany) and a daily diary where all physical activities were additionally documented. All study procedures were approved by the local ethics committee of Hannover Medical School (Vote #7617) and all subjects provided informed written consent prior to the commencement of the study procedures.

Mice study: Mice with a cardiomyocyte-restricted knockout of STAT3 (CKO: aMHC-Cre$^{tg/+}$; STAT3$^{flox/flox}$) and wildtype mice (WT: STAT3$^{flox/flox}$) were used to analyze the effect of an altered androgen receptor signaling in male mice for cardiac PGE2 secretion and modulation of the immune response. Application of the COX inhibitor ibuprofen as therapeutic strategy was tested.

Mice were housed in a specific pathogen-free barrier facility and fed standard chow. All animal studies were conducted in accordance with the German animal protection legislation and with the European Communities Council Directives 86/609/EEC and 2010/63/EU for the protection of animals used for experimental purposes. All experiments were approved by the Local Institutional Animal Care and Research Advisory Committee and permitted by the relevant local authority for animal protection "Niedersächisisches Landesamt für Verbrauerschutz und Lebensmittelsicherheit" (LAVES).

Blood sampling and blood tests

Blood samples were collected in S-Monovette® tubes containing ethylenediaminetetraacetic acid (EDTA, for plasma) or clot activator (for serum) at the time of hospitalization or at study inclusion (baseline, BL) and at the follow-up (FU) visits after 12 months for the Rebirth 60Plus male and female subjects (age >60 years). Blood samples were also obtained from young male and female subjects (age 18-50 years) from

a healthy population established by Hannover Unified Biobank (HUB). Plasma or serum was separated by centrifugation at 1500 rpm for 10 min and aliquots were stored at -80 °C. Laboratory workup was performed as part of routine analysis by hospital laboratories for leukocytes, neutrophils, lymphocytes, platelets, CRP and LDH. PGE2 serum and plasma levels were measured using the prostaglandin E2 ELISA kit (abcam ab133021) according to the manufacturer's protocol. Since the PGE2 ELISA system used in the study is suitable for research use only and is not intended for diagnostic use, we showed relative PGE2 expression in %. IL-17A serum levels were measured using the IL-17A ELISA kit (abcam ab216167).

Infection of Calu-3 cells with SARS-CoV-2 and taxifolin treatment

Calu-3 cells (kindly provided by Prof. Pöhlmann, German Primate Center, Göttingen; ATCC Cat# HTB-55; RRID:CVCL_0609) were maintained in Dulbecco's' modified Eagle medium and Vero cells (ATCC-CCL-81; Lot 58484194) in Advanced MEM at 37°C and 5% CO_2. Both media were supplemented with 10% fetal bovine serum, 2 mM glutamine, 0.1 mM non-essential amino acids and 1% Penicillin/Streptomycin. Calu-3 cells ($4.5x10^5$ cells/well) were seeded in collagen-coated 24-well plates. For infection, the SARS-CoV-2 (strain SARS-CoV-2/München-1.2/2020/984,p3) [31] kindly provided by Christian Drosten (Charité, Berlin) through the European Virus Archive – Global (EVAg) was used. The isolate was propagated and titrated in Vero cells. Calu-3 cells were pretreated with 100 µM taxifolin or DMSO (0.15 %) for 24 h. Infection with SARS-CoV-2 isolate was performed at a MOI of $2.0x10^{-5}$ for 4 h at 37°C in the presence of the compounds. Heat-inactivated virus (15 min, 70°C) served a negative control. After infection, cells were washed twice with PBS before the medium containing the respective compound was added. At 48 h post infection, culture supernatant was collected and heat-inactivated (15 min, 70°C) prior to the detection of PGE2. RNA was isolated from cell lysates using a NucleoSpin RNA kit (Macherey-Nagel) according to the manufacturer's instructions to analyze virus genome copy numbers, COX-2 and HPGD expression.

Quantification of SARS-CoV-2 viral load in Calu-3 cells

Viral RNA was isolated from lysates by NucleoSpin RNA kit (Macherey-Nagel) and from supernatant samples by QIAamp Viral RNA Mini Kit (Qiagen) according to the manufacturer's guidelines. RT-qPCR was performed in duplicates using a LightCycler 480 (Roche) based on a method described previously[25]. Viral copy numbers were determined against a standard provided by Sven Reiche (FLI, Germany). Each biological replicate consisted of an average of between two and four samples, each analyzed by RT-qPCR in duplicate Data were transformed by y=log(y).

Virus titration in Vero E6 cells for infection of lung slices with SARS-CoV-2

Vero E6 (ATCC CRL-1586) and Vero cells (ATCC CCL-81) were maintained in Eagle's Minimum Essential Medium (EMEM) (Lonza) supplemented with 25 mM of HEPES (Gibco), 1 × GlutaMAX (Gibco), 100 U/ml penicillin and 100 µg/ml streptomycin. SARS-CoV2 isolate (strain SARS-CoV-2/München-1.2/2020/984,p3) [31] was kindly provided by Christian Drosten. SARS-CoV-2 seed stocks were generated by inoculating Vero E6 (ATCC CRL-1586) at a multiplicity of infection (moi) of 0.001, collecting and

aliqouting the culture supernatant at 72 h post infection (hpi), then storing at -80°C in aliquots. SARS-CoV-2 working stocks were generated by an additional passage on Vero cells (ATCC CCL-81) at a moi of 0.001. Plaque and median tissue culture infectious dose ($TCID_{50}$) assays were performed to titrate the cultured virus after both passages using Vero cells. This stock was used for the *ex vivo* infections of human tissues.

Infections of precision-cut human lung slices (PCLS) with SARS-CoV-2

PCLS were maintained in DMEM/F12 medium (Gibco, Thermo Fisher Scientific) supplemented with 2 mM of HEPES (Gibco), 1 × GlutaMAX (Gibco), 100 U/ml penicillin and 100 µg/ml streptomycin; this media was also used for virus dilutions and post-infection incubation. On the day of infection, PCLS were rinsed with PBS (without Mg^{2+} and Ca^{2+}) then inoculated with 1×10^5 PFU SARS-CoV-2 in 250 µl of media per well in 48-well plates and incubated at 37°C. After 2 h, the inoculum was removed and the PCLS were then cultured in 250 µl of DMEM/F12 medium. At 72 and 120 hpi, supernatants were collected and PCLS were fixed with fixation buffer (4% PFA, 0.1% glutaraldehyde and 200 mM HEPES in ddH_2O) for 1 h at room temperature followed by 24 h at 4°C.

QRT-PCR for NSP7 to confirm SARS-CoV-2 infection

SARS-CoV-2 infections in human Calu-3 cells and human lung slices and tissue were verified by NSP7 mRNA expression using qRT-PCR (forward primer: GGG CTC AAT GTG TCC AGT TAC, reverse primer: TTG CCC TGT TGT CCA GCA TT).

Multiplex immunohistochemistry of human lung biopsies

The FFPE sections for each group (Control (Ctrl) n=3, acute COVID-19 (AC) n=6, transplant rejected (TR) n=4) were representatively stained with the manual Opal 7-Color IHC Kit (Akoya Biosciences, Marlborough, MA) as previously described [59]. The primary antibodies CD4 (Cytomed SP35, 1:50), CD8 (Dako M0755, 1:600), CD68 (Dako PGM1, 1:750) and CD20 (Dako M0755, 1:1000) were combined in sequence with the opal fluorophore CD4-Opal520, CD8-Opal570, CD20-Opal540 and CD68-Opal650. The sections were scanned with the Vectra 3 System (Akoya Biosciences, Marlborough, MA). The Regions of Interest (ROIs) were selected representative for small, medium and large vessels for the entire tissue section. The number of analyzed stamps was 43 for Ctrl, 74 for AC and 56 for TR. For the detection of $CD20^+$ B cells, the analysis was performed with the inForm Advanced Image Analysis Software Version 2.3.0 (Akoya Biosciences, Marlborough, MA) and ImageJ 1.53c (Wayne Rasband, National Institutes of Health, USA). Statistical analysis was performed using the generalized linear model with Gaussian distribution and weights adjusted according to the number of ROIs per patient.

Stimulation of human pre-B-cell lines

Human pre-B-cell lines 697 (ACC42 DSMZ collection) and SUP-B15 (ACC389 DSMZ collection) were cultivated in RPMI (Gibco) supplemented with 10 % FBS. $5x10^5$ cells per ml were pre-incubated with either

the EP1/EP2 receptor antagonist AH6809 (10 µM, Tocris) or the EP4 receptor antagonist GW627368 (10 µM, Tocris) for 2 h. PGE2 (10 µM, Sigma-Aldrich) was added and cells were harvested after 48 h in TRIzol. Control cells were incubated with dissolvents (DMSO or ethanol (ETHO), 1 µL/ml media). Alternatively, $5x10^5$ per ml 697 and SUP-B15 cells were incubated with 10 % human serum from older individuals (>60 y) prior to the commencement of the exercise program at baseline (BL) and after 12M (12M FU) for 48 h and harvested in TRIzol SUP-B15 cells were incubated with 10 % human serum from COVID-19 patients and from healthy controls. Cells were harvested after 48 h in TRIzol

DEP characteristics

Diesel exhaust particles (DEP, SRM 2975, industrial forklift) were purchased from the National Institute of Standards and Technology (NIST, Gaithersburg, MD, USA). A list of the polycyclic aromatic hydrocarbons (PAHs) concentrations and characteristics of the particles in SRM 2975 are available on NIST website (http://www.nist.gov/srm/).

For *in vitro* experiments, DEP was suspended in 2mg/ml PBS, vortexed and sonicated for 2 minutes by probe sonication and filtered by 5 mm sterifix filter (Braun). Just before use, the particles were resonicated for 15 min in a bath sonicator [60].

Isolation and cultivation of adult human cardiac endothelial cells (hCECs)

hCECs were isolated from atrial appendages. Surrounding fat tissue was removed from the atrial appendage, the cardiac tissue was mechanically and subsequently enzymatically dissociated using the Neonatal Rat Heart Dissociating Kit (Miltenyi) according to the manufacturer's instructions. Dissociated single cells were cultured in EGM-2 (Lonza). For the enrichment of hCECs, the human CD31 Microbead Kit (Miltenyi Biotec) was used according to the manufacturer's instructions and cultivated in EGM-2. Cells were used from passage 3-6 [61].

hCECs were incubated with 10 mg/ml DEP and/or 100 mM taxifolin for 24 h in EGM-2+supplements bullet kit (Lonza CC-3162) media in a humidified incubator at 37 °C and 5% CO_2. hCECs control cells received equal amounts of PBS and/or DMSO.

PGE2 detection in supernatants of Calu-3, hCEC and murine adult cardiomyocytes

PGE2 levels in the supernatants of the primary hCEC (normalized to cell density), murine adult cardiomyocytes (normalized to aMHC mRNA expression), and the cell lines Calu-3 (normalized to total RNA content) were measured using the prostaglandin E2 ELISA kit (abcam ab133021) respectively, according to the manufacturer's protocols.

Isolation of RNA and qRT-PCR

Total RNA was isolated with TRIzol (Thermo Fisher Scientific) and cDNA synthesis was performed as described previously [62]. Real-time PCR with the SYBR green dye method (Brilliant SYBR Green Mastermix-

Kit, Thermo Fisher Scientific) was performed with the AriaMx Real-Time PCR System (Agilent Technologies) as described [62]. Expression of mRNA levels was normalized using the 2-ΔΔCT method relative to 18S, B2M and GAPDH. A list of qRT-PCR primers used in this study is provided in the supplements file Table S1, S2.

RNA Isolation from formalin fixed and paraffin embedded tissue

RNA isolation from formalin-fixed and paraffin embedded tissue was performed using the Maxwell® RSC RNA FFPE Purification Kit (Promega Corporation, Madison, WI). RNA content was measured by using the Qubit RNA IQ Assay (Thermo Fisher Scientific, Waltham, MA).

Isolation, characterization and culture of Sca-1^{+} cardiac progenitor cells

Mice with a cardiomyocyte-restricted knockout of STAT3 (CKO: aMHC-Cre$^{tg/+}$; STAT3$^{flox/flox}$) and wildtype mice (WT: STAT3$^{flox/flox}$) were generated and isolation and cultivation of Sca-1 cardiac progenitor cells from hearts of 3 month-old mice was performed as described [63] [39]. Isolated WT-CPC were incubated with PGE2 (1 µM) for 48 h and were harvested in TRIzol.

Male CKO mice at the age of 9-10 weeks were treated with ibuprofen (10 mg/kg bodyweight, ibuprofen sodium salt, Sigma-Aldrich, dissolved in drinking water) for two weeks [39]. CKO control animals received drinking water.

Freshly isolated Sca-1 positive CPC were stained with CD19-PE (BD Pharmingen, 557399) for 15 min at room temperature. Flow cytometry was performed using the FACSCalibur (BD Biosciences).

Immunostaining

For immunostainings using antibodies recognizing CD19 (CD19-PE, BD Pharmingen, 557399) and Sca-1 (Sca-1-FITC microbead kit, Miltenyi Biotec), cryosections were fixed in acetone, washed 3 times with PBS and blocked with 10 % donkey serum and 0.3 % Triton in PBS for 1 h at room temperature. Cryosections were stained with the antibodies for 2 h at room temperature. Nuclei were stained with DAPI Hoechst 33342 (Sigma-Aldrich). Images were acquired with Axio Observer 7 and Zen 2.6 pro software (Carl Zeiss).

Statistical Analyses

Statistical analysis was performed using GraphPad Prism version 5.0a, 7.0 and 8.1.2 for Mac OS X (GraphPad Software, San Diego, CA, USA).

Normal distribution was tested using the D'Agostino normality test. Continuous data were expressed as mean ± SD or median and interquartile range (IQR), according to the normality of distribution. Comparison between two groups was performed using one sample *t*-test or unpaired two-tailed t-test for Gaussian distributed data and the Mann-Whitney-U test where at least one column was not normally distributed. When comparing more than two groups, ANOVA and Bonferroni's post hoc test or Dunnett's

post hoc test were used according to the normality of distribution. Categorical variables are presented as frequencies (percentages) and compared using Fisher's exact test. A two-tailed *P* value of <0.05 was considered statistically significant. Correlation for BMI, BW, body fat content and age was analyzed via ozone correlation analysis by using Pearson correlation coefficients for Gaussian distributions or for nonparametric Spearman correlation coefficients for non-normal distribution.

Declarations

Acknowledgments: We thank Sergej Erschow, Silvia Gutzke, Brigit Brandt, Angelica Julieth Diaz Basabe, Delphine De Mulder, Thomas Gerlach and Giulietta Saletti for excellent technical assistance, and Dr. Helge Stark for the bioinformatic analysis input. The SARS-CoV-2 virus was kindly provided by Christian Drosten, Charité, Berlin.

Funding: This work was supported by:

The German Research Foundation [DFG, HI 842/3-2 to D.H.-K.], by the DFG Clinical Research Group [DFG KFO311, HI 842/10-1, HI 842/10-2 to D.H.-K.RI 2531/2-1, RI 2531/2-2 to M.R.-H.], by REBIRTH I/II to D.H.-K., DFG as part of the German Strategy for Excellence [EXC 2155 "RESIST", Project ID 39087428], The DEFEAT PANDEMIcs (AP6-9, DJ, MK), by the (DFG – Projektnummer 158989968 - SFB 900 project C7 and DFG project GE 2145/3-2), the Ministry of Lower Saxony (MWK, project 76251-99-3/19), The European Research Council Consolidator Grant (XHale; 771883)

The Knut and Alice Wallenberg Foundation. The European Virus Archive GLOBAL (EVA-GLOBAL) project funded by the European Union's Horizon 2020 research and innovation program under grant agreement No 871029 (to Christian Drosten). This work was partly supported by the Alexander von Humboldt Foundation in the framework of the Alexander von Humboldt Professorship endowed by the German Federal Ministry of Education and Research and by funding from the Ministry for Science and Culture (MWK), Lower Saxony, Germany (14 - 76103-184 CORONA-15/20 to GFR). APG was supported by the Deutsches Zentrum für Infektionsforschung (DZIF; German Center for Infection Research; Grant No. TTU 05.816 00 to T.P.). Work by JLB was supported by grants from Fonds National de la Recherche Scientifique (FNRS) and WEBIO. JLB is an established investigator of the WELBIO institute.

Author contributions:

MRH - Conceptualization, methodology, validation, formal analysis, investigation, data curation, writing - original draft preparation, writing- review & editing, visualization, supervision, project administration, funding acquisition

ES - Conceptualization, methodology, validation, formal analysis, investigation, data curation, writing - original draft preparation, writing- review & editing, visualization

LW - Methodology, investigation, resources, writing - original draft preparation

APG - Methodology, investigation, resources, writing - original draft preparation

MK - Data curation

FJZ-B - Methodology, investigation, resources, writing- review & editing

GB - Methodology, formal analysis, investigation, resources, writing- review & editing, visualization

GG - Methodology, validation, formal analysis, investigation, resources, writing - review & editing, supervision, project administration, funding acquisition

KB - Data curation, visualization

TP - Conceptualization, methodology, writing- review & editing, supervision, funding acquisition

VM - Resources, writing- review & editing

J-LB - Resources, writing- review & editing

FF – Investigation, resources

EH - Conceptualization, resources

HE - Methodology, investigation, writing - original draft preparation, writing- review & editing

GFR - Investigation, writing- review & editing, funding acquisition

AH - Methodology, validation, formal analysis, investigation, resources, data curation, writing - original draft preparation, writing- review & editing, visualization

MPK - Resources, writing - original draft preparation, writing- review & editing, supervision,

DJ - Conceptualization, methodology, validation, formal analysis, investigation, resources, data curation, writing - original draft preparation, writing- review & editing, visualization, supervision, project administration, funding acquisition

JE - Investigation, data curation, writing- review & editing, project administration

UT - Conceptualization, investigation, resources, writing- review & editing, project administration

LM - Investigation, resources, data curation, writing- review & editing,

MS - Data curation, visualization

TI - Methodology, resources, writing - review & editing, funding acquisition

AS - Conceptualization, writing- review & editing

TJP - Investigation, resources, data curation, writing- review & editing

BA - Methodology

AH – Methodology, resources, editing

AH - Conceptualization, methodology, investigation, resources, writing- review & editing

DHK - Conceptualization, methodology, validation, formal analysis, investigation, data curation, writing - original draft preparation, writing- review & editing, visualization, supervision, project administration, funding acquisition

Competing interests: None of the authors have any conflicts of interest or financial interests to declare.

Data and materials availability:

The SARS-CoV-2 virus was kindly provided by Christian Drosten, Charité, Berlin.

References

1. Lau MSY, Grenfell B, Thomas M, Bryan M, Nelson K, Lopman B. Characterizing superspreading events and age-specific infectiousness of SARS-CoV-2 transmission in Georgia, USA. *Proc Natl Acad Sci U S A* **117**, 22430-22435 (2020).

2. Vardhana SA, Wolchok JD. The many faces of the anti-COVID immune response. *The Journal of experimental medicine* **217**, (2020).

3. Fried JA*, et al.* The Variety of Cardiovascular Presentations of COVID-19. *Circulation* **141**, 1930-1936 (2020).

4. Ackermann M*, et al.* Pulmonary Vascular Endothelialitis, Thrombosis, and Angiogenesis in Covid-19. *N Engl J Med* **383**, 120-128 (2020).

5. Yin S, Huang M, Li D, Tang N. Difference of coagulation features between severe pneumonia induced by SARS-CoV2 and non-SARS-CoV2. *J Thromb Thrombolysis*, (2020).

6. Zheng YY, Ma YT, Zhang JY, Xie X. COVID-19 and the cardiovascular system. *Nature reviews Cardiology*, (2020).

7. Zheng Z*, et al.* Risk factors of critical & mortal COVID-19 cases: A systematic literature review and meta-analysis. *J Infect*, (2020).

8. Nicolai L*, et al.* Immunothrombotic Dysregulation in COVID-19 Pneumonia Is Associated With Respiratory Failure and Coagulopathy. *Circulation* **142**, 1176-1189 (2020).

9. Szekely Y*, et al.* Spectrum of Cardiac Manifestations in COVID-19: A Systematic Echocardiographic Study. *Circulation* **142**, 342-353 (2020).

10. Chen L, Li X, Chen M, Feng Y, Xiong C. The ACE2 expression in human heart indicates new potential mechanism of heart injury among patients infected with SARS-CoV-2. *Cardiovasc Res* **116**, 1097-1100 (2020).

11. Fox SE*, et al.* Unexpected Features of Cardiac Pathology in COVID-19 Infection. *Circulation* **142**, 1123-1125 (2020).

12. Sharma A*, et al.* Human iPSC-Derived Cardiomyocytes Are Susceptible to SARS-CoV-2 Infection. *Cell Rep Med* **1**, 100052 (2020).

13. Wenham C, Smith J, Morgan R, Gender, Group C-W. COVID-19: the gendered impacts of the outbreak. *Lancet* **395**, 846-848 (2020).

14. Brandt EB, Beck AF, Mersha TB. Air pollution, racial disparities, and COVID-19 mortality. *J Allergy Clin Immunol* **146**, 61-63 (2020).

15. Martelletti L, Martelletti P. Air Pollution and the Novel Covid-19 Disease: a Putative Disease Risk Factor. *SN Compr Clin Med*, 1-5 (2020).

16. Li D*, et al.* Immune dysfunction leads to mortality and organ injury in patients with COVID-19 in China: insights from ERS-COVID-19 study. *Signal Transduct Target Ther* **5**, 62 (2020).

17. Wilk AJ*, et al.* A single-cell atlas of the peripheral immune response in patients with severe COVID-19. *Nat Med* **26**, 1070-1076 (2020).

18. Quinti I*, et al.* A possible role for B cells in COVID-19? Lesson from patients with agammaglobulinemia. *J Allergy Clin Immunol*, (2020).

19. Kaneko N*, et al.* Loss of Bcl-6-Expressing T Follicular Helper Cells and Germinal Centers in COVID-19. *Cell*, (2020).

20. Catanzaro M, Fagiani F, Racchi M, Corsini E, Govoni S, Lanni C. Immune response in COVID-19: addressing a pharmacological challenge by targeting pathways triggered by SARS-CoV-2. *Signal Transduct Target Ther* **5**, 84 (2020).

21. Hu B, Huang S, Yin L. The cytokine storm and COVID-19. *J Med Virol*, (2020).

22. Mehta P*, et al.* COVID-19: consider cytokine storm syndromes and immunosuppression. *Lancet* **395**, 1033-1034 (2020).

23. Wang SF*, et al.* Antibody-dependent SARS coronavirus infection is mediated by antibodies against spike proteins. *Biochemical and biophysical research communications* **451**, 208-214 (2014).

24. Zhang Q*, et al.* Inborn errors of type I IFN immunity in patients with life-threatening COVID-19. *Science* **370**, (2020).

25. Sander WJ, O'Neill HG, Pohl CH. Prostaglandin E2 As a Modulator of Viral Infections. *Front Physiol* **8**, 89 (2017).

26. Coulombe F*, et al.* Targeted prostaglandin E2 inhibition enhances antiviral immunity through induction of type I interferon and apoptosis in macrophages. *Immunity* **40**, 554-568 (2014).

27. Full F, Gack MU. Prostaglandin E2: the villain in the host response to influenza virus. *Immunity* **40**, 453-454 (2014).

28. Liu L*, et al.* Influenza A virus induces interleukin-27 through cyclooxygenase-2 and protein kinase A signaling. *J Biol Chem* **287**, 11899-11910 (2012).

29. Schmidleithner L*, et al.* Enzymatic Activity of HPGD in Treg Cells Suppresses Tconv Cells to Maintain Adipose Tissue Homeostasis and Prevent Metabolic Dysfunction. *Immunity* **50**, 1232-1248 e1214 (2019).

30. Hoxha M. What about COVID-19 and arachidonic acid pathway? *Eur J Clin Pharmacol* **76**, 1501-1504 (2020).

31. Wolfel R*, et al.* Virological assessment of hospitalized patients with COVID-2019. *Nature* **581**, 465-469 (2020).

32. Khailany RA, Safdar M, Ozaslan M. Genomic characterization of a novel SARS-CoV-2. *Gene Rep* **19**, 100682 (2020).

33. Hamalainen M, Nieminen R, Asmawi MZ, Vuorela P, Vapaatalo H, Moilanen E. Effects of flavonoids on prostaglandin E2 production and on COX-2 and mPGES-1 expressions in activated macrophages. *Planta Med* **77**, 1504-1511 (2011).

34. Wang Y*, et al.* Taxifolin prevents beta-amyloid-induced impairments of synaptic formation and deficits of memory via the inhibition of cytosolic phospholipase A2/prostaglandin E2 content. *Metab Brain Dis* **33**, 1069-1079 (2018).

35. Soleymani Fard S, Jeddi Tehrani M, Ardekani AM. Prostaglandin E2 induces growth inhibition, apoptosis and differentiation in T and B cell-derived acute lymphoblastic leukemia cell lines (CCRF-CEM and Nalm-6). *Prostaglandins Leukot Essent Fatty Acids* **87**, 17-24 (2012).

36. Chen R*, et al.* PGE2 ameliorated viral myocarditis development and promoted IL-10-producing regulatory B cell expansion via MAPKs/AKT-AP1 axis or AhR signaling. *Cell Immunol* **347**, 104025 (2020).

37. Boniface K*, et al.* Prostaglandin E2 regulates Th17 cell differentiation and function through cyclic AMP and EP2/EP4 receptor signaling. *The Journal of experimental medicine* **206**, 535-548 (2009).

38. Lee J, Aoki T, Thumkeo D, Siriwach R, Yao C, Narumiya S. T cell-intrinsic prostaglandin E2-EP2/EP4 signaling is critical in pathogenic TH17 cell-driven inflammation. *J Allergy Clin Immunol* **143**, 631-643 (2019).

39. Stelling E*, et al.* Increased prostaglandin-D2 in male but not female STAT3-deficient hearts shifts cardiac progenitor cells from endothelial to white adipocyte differentiation. *PLOS Biol*, (2020).

40. Davies NG*, et al.* Age-dependent effects in the transmission and control of COVID-19 epidemics. *Nat Med* **26**, 1205-1211 (2020).

41. Schmidt LM*, et al.* Bronchial epithelial cell-derived prostaglandin E2 dampens the reactivity of dendritic cells. *J Immunol* **186**, 2095-2105 (2011).

42. Zhao Y*, et al.* Regulation of COX-2 expression and IL-6 release by particulate matter in airway epithelial cells. *Am J Respir Cell Mol Biol* **40**, 19-30 (2009).

43. Delogu A, Schebesta A, Sun Q, Aschenbrenner K, Perlot T, Busslinger M. Gene repression by Pax5 in B cells is essential for blood cell homeostasis and is reversed in plasma cells. *Immunity* **24**, 269-281 (2006).

44. Schebesta A, McManus S, Salvagiotto G, Delogu A, Busslinger GA, Busslinger M. Transcription factor Pax5 activates the chromatin of key genes involved in B cell signaling, adhesion, migration, and immune function. *Immunity* **27**, 49-63 (2007).

45. Nutt SL, Tarlinton DM. Germinal center B and follicular helper T cells: siblings, cousins or just good friends? *Nat Immunol* **12**, 472-477 (2011).

46. Simkin NJ, Jelinek DF, Lipsky PE. Inhibition of human B cell responsiveness by prostaglandin E2. *J Immunol* **138**, 1074-1081 (1987).

47. Murn J, Alibert O, Wu N, Tendil S, Gidrol X. Prostaglandin E2 regulates B cell proliferation through a candidate tumor suppressor, Ptger4. *The Journal of experimental medicine* **205**, 3091-3103 (2008).

48. Schultheiss C*, et al.* Next-Generation Sequencing of T and B Cell Receptor Repertoires from COVID-19 Patients Showed Signatures Associated with Severity of Disease. *Immunity* **53**, 442-455 e444 (2020).

49. Johnson K, Shapiro-Shelef M, Tunyaplin C, Calame K. Regulatory events in early and late B-cell differentiation. *Mol Immunol* **42**, 749-761 (2005).

50. Iwasaki A. What reinfections mean for COVID-19. *Lancet Infect Dis*, (2020).

51. Tillett RL*, et al.* Genomic evidence for reinfection with SARS-CoV-2: a case study. *Lancet Infect Dis*, (2020).

52. Lancman G, Mascarenhas J, Bar-Natan M. Severe COVID-19 virus reactivation following treatment for B cell acute lymphoblastic leukemia. *J Hematol Oncol* **13**, 131 (2020).

53. Sajiki Y*, et al.* Prostaglandin E2-Induced Immune Exhaustion and Enhancement of Antiviral Effects by Anti-PD-L1 Antibody Combined with COX-2 Inhibitor in Bovine Leukemia Virus Infection. *J Immunol* **203**, 1313-1324 (2019).

54. Tang T*, et al.* Macrophage responses to lipopolysaccharide are modulated by a feedback loop involving prostaglandin E2, dual specificity phosphatase 1 and tristetraprolin. *Sci Rep* **7**, 4350 (2017).

55. Agard M, Asakrah S, Morici LA. PGE(2) suppression of innate immunity during mucosal bacterial infection. *Front Cell Infect Microbiol* **3**, 45 (2013).

56. Qaseem A, Horwitch CA, Vijan S, Etxeandia-Ikobaltzeta I, Kansagara D, Clinical Guidelines Committee of the American College of P. Testosterone Treatment in Adult Men With Age-Related Low Testosterone: A Clinical Guideline From the American College of Physicians. *Ann Intern Med* **172**, 126-133 (2020).

57. Zhang Y*, et al.* Management of heart failure patients with COVID-19: a joint position paper of the Chinese Heart Failure Association & National Heart Failure Committee and the Heart Failure Association of the European Society of Cardiology. *Eur J Heart Fail* **22**, 941-956 (2020).

58. André F, Manuel S, Santhosh N, Markus A. L, Martin S. *Inhibitors for Novel Coronavirus Protease Identified by Virtual Screening of 687 Million Compounds* (2020).

59. Mascaux C*, et al.* Immune evasion before tumour invasion in early lung squamous carcinogenesis. *Nature* **571**, 570-575 (2019).

60. Labranche N, Khattabi CE, Berkenboom G, Pochet S. Effects of diesel exhaust particles on macrophage polarization. *Hum Exp Toxicol* **36**, 412-420 (2017).

61. Manikowski D*, et al.* Human adipose tissue-derived stromal cells in combination with exogenous stimuli facilitate three-dimensional network formation of human endothelial cells derived from various sources. *Vascul Pharmacol* **106**, 28-36 (2018).

62. Hoch M*, et al.* Erythropoietin preserves the endothelial differentiation capacity of cardiac progenitor cells and reduces heart failure during anticancer therapies. *Cell Stem Cell* **9**, 131-143 (2011).

63. Hilfiker-Kleiner D*, et al.* Signal transducer and activator of transcription 3 is required for myocardial capillary growth, control of interstitial matrix deposition, and heart protection from ischemic injury. *Circ Res* **95**, 187-195 (2004).

Table

Table 1. Summary of clinical data of the COVID-19 patients

Parameters	COVID-19 patients total (N=89)	Mild to moderate disease COVID-19 disease (N=41)	Severe COVID-19 disease (N=48)
Age (years, median ± IQR)	59 (46-68)	51 (40-67)	62 (51-68.75)*
Sex female (%)	30% (27/89)	44% (18/41)	19% (9/48)*
Body weight (kg, median ± IQR)	79.5 (67.75-96.5) (n=42)	75 (65.5-86.5) (n=25)	90 (76-100)* (n=17)
Body height (cm, mean ± SD)	171.9±9.4 (n=43)	170±9.28 (n=25)	174.6±9.1 (n=18)
BMI (median ± IQR)	27.2 (23.7-30.2) (n=43)	26.56 (22.96-28.9) (n=26)	28 (25.5-31.95) (n=17)
Diabetes (%)	28% (11/50)	19% (5/26)	25% (6/24)
Total leucocytes, counts/µl (mean ± SD) Standard value: 3900-10200 counts/µl	8036±5831 (n=50)	6803±3213 (n=26)	9373±7592 (n=24)
Neutrophils, counts/µl (mean ± SD) Standard value: 1500-7700 counts/µl	4999±2697 (n=35)	4664±2614 (n=21)	5502±2839 (n=14)
Lymphocytes, counts/µl (mean ± SD) Standard value: 1100-4500 counts/µl	1114±564 (n=36)	1266±608 (n=21)	902±428 (n=15)
CRP mg/L (mean ± SD) Standard value: <5 mg/L	107±83 (n=50)	69.4±55.95 (n=26)	147.1±89*** (n=24)
LDH at hospitalization UI/L (median ± IQR) Standard value: <248 UI/L	363.5 (263.8-518.8) (n=48)	299 (229-375) (n=25)	459 (348-659)*** (n=23)
Platelets at hospitalization 10^3/µl (mean ± SD)	229±81 (n=50)	235±80 (n=26)	221±83 (n=24)

Standard value: 160-370 10^3/µl			
Mortality (%)	15% (13/89)	0% (0/41)	27% (13/48)***

Body mass index (BMI), C-reactive protein (CRP), lactate dehydrogenase (LDH), leukocytes normal count, neutrophils normal count, and lymphocytes below normal counts, were analyzed at the time of hospitalization in routine clinical lab tests. Standard values of blood parameters were indicated in the parameter column. Values outside the normal range were indicated in red. Comparison between the groups of mild and severe COVID-19 was performed using Student's t-test for Gaussian distributed data (presented as mean ± SD) and the Mann-Whitney-U test where at least one column was not normally distributed (presented as median and interquartile range (IQR)). Categorical variables are presented as frequencies (percentages) and were compared using Fisher's exact test. *P<0.05, **P<0.01, ***P<0.001 severe COVID-19 vs mild to moderate COVID-19 disease.

Figures

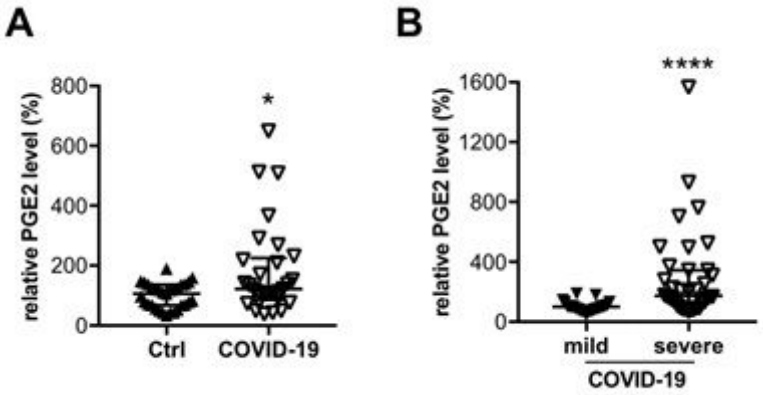

Figure 1

Circulating PGE2 levels are elevated in COVID-19 patients. (A) The dot plots summarize relative circulating serum PGE2 levels (in %) of COVID-19 patients (n=29) and healthy controls (n=31); the median of healthy controls was set at 100 %. (B) The dot plots summarize relative circulating plasma PGE2 levels (in %) of patients with severe (n=36) and mild (n=24) disease; the median of patients with mild disease was set at 100 %. (A-B) Data are presented as median IQR, *P<0.05, **P<0.01, ****P<0.0001, Mann-Whitney-U test.

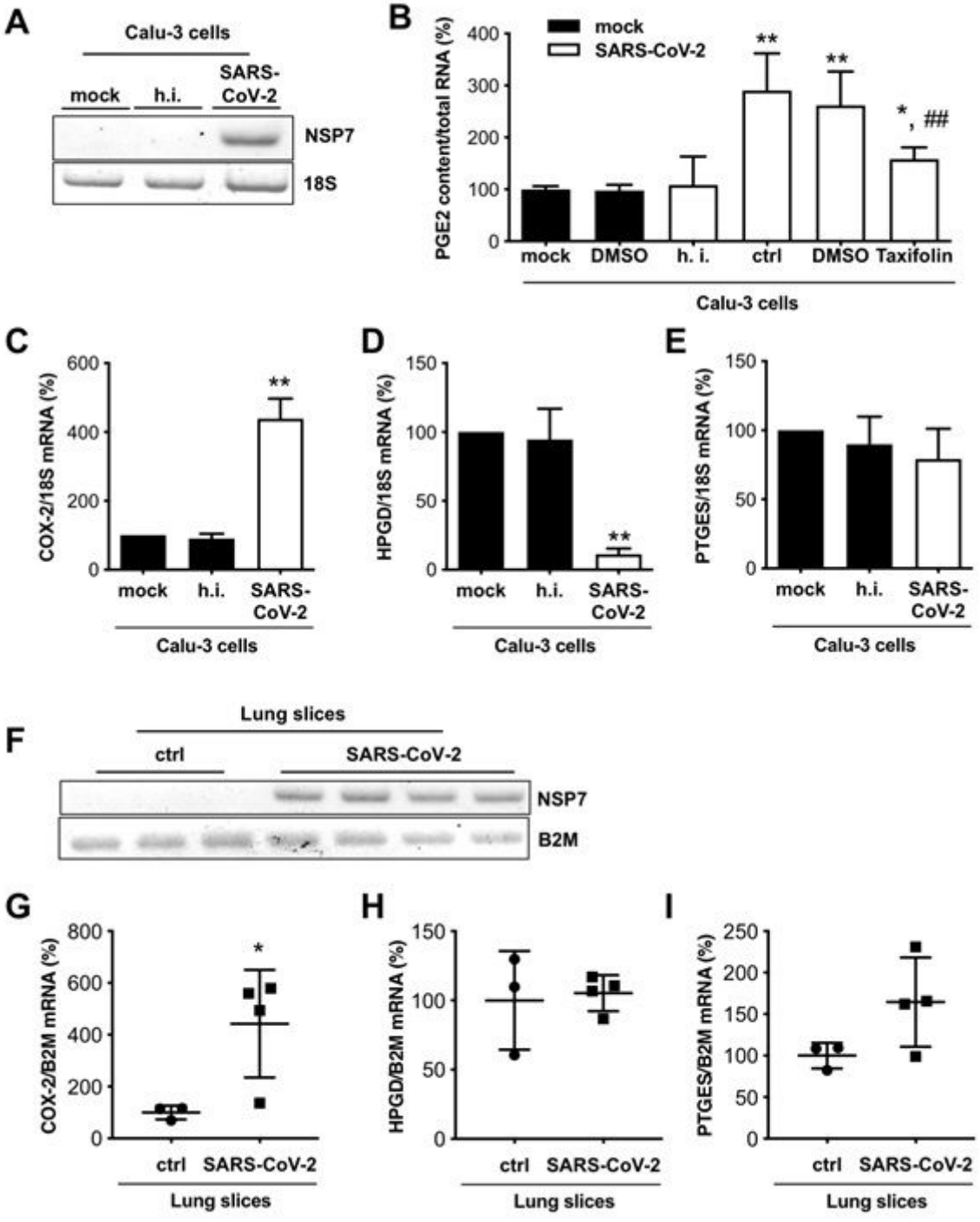

Figure 2

SARS-CoV-2 infection modulates PGE2 secretion and COX-2 and HPGD expression. (A) Representative gel image of NSP7 mRNA expression of Calu-3 cells infected with SARS-CoV-2 and control cells. (B) The bar graph summarizes PGE2 content in supernatants of Calu-3 cells infected with SARS-CoV-2 and treated with taxifolin (n= 4) compared with untreated mock (n= 6), DMSO control (n= 8) and heat-inactivated (h.i.) SARS-CoV2 (n= 6). The bar graphs summarize mRNA expressions of (C) COX-2, (D) HPGD and (E) PTGES of SARS-CoV-2 infected Calu-3 cells (n=3). (F) Representative gel image of NSP7 and B2M mRNA

expression of SARS-CoV-2 infected lung slices and control slices. The bar graphs summarize mRNA expressions of (G) COX-2, (H) HPGD and (I) PTGES of SARS-CoV-2 infected lung slices (n=3 for ctrl, n=4 for SARS-CoV-2 infection). Data are presented as mean±SD, (B) unpaired two-tailed t-test, *P<0.05 vs. mock, **P<0.01 vs. mock, ##P<0.01 vs. SARS-CoV-2 + DMSO. (C-E) One sample t-test, *P<0.05, **P<0.01 vs. ctrl, (G-I) unpaired two-tailed t-test, *P<0.05 vs. ctrl.

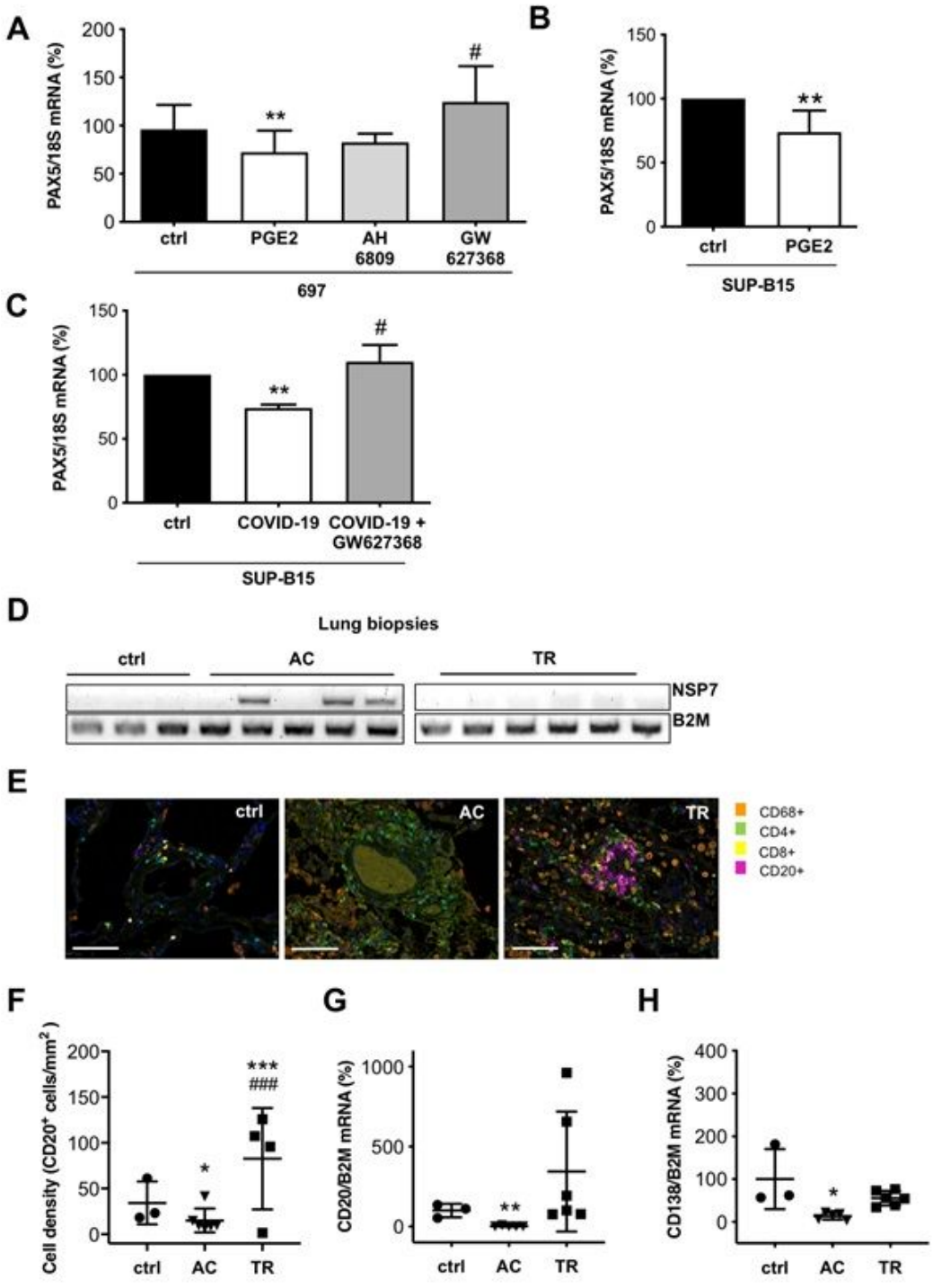

Figure 3

PGE2 stimulation of B-cells modulates the immune response. (A) The bar graph summarizes PAX5 mRNA expression of 697 pre-B-cells treated with AH6809 (10 µM) or GW627368 (10 µM) and PGE2 (10 µM) for 48 h (n=18 for ctrl and PGE2 treated cells, n=3 for AH6809 treated cells and n=6 for GW627368 treated cells). (B) The bar graph summarizes PAX5 mRNA expression of human pre-B-cell line SUP-B15 with PGE2 (10 µM) for 48 h (n= 9). (C) The bar graph summarizes PAX5 mRNA expression of SUP-B15 pre-B-cells treated with serum from healthy controls (serum pooled from 9 controls) and from COVID-19 patients (serum pooled from 9 COVID-19 patients) incubated with and without GW627368 (10 µM). Control cells were treated with the solvent DMSO (n=6 wells with control serum and n=3 wells with serum of COVID-19 patients with and without GW627368). (D) Representative gel image of NSP7 and B2M mRNA expression in control lung tissue (ctrl), in lung tissue of patients with severe acute COVID-19 disease (AC) and in lung tissue obtained after transplant rejection (TR). (E) Immunohistochemical staining for CD68+, CD4+, CD8+ and CD20+ immune cells (scale bar: 100 µm), (F) Dot plot summarizing the immunohistological quantification of CD20 positive B-cells per area (mm), dot plots summarize mRNA expression of (G) CD20 and (H) of CD138 in control lung tissue (ctrl), in the lung tissue of patients with severe acute COVID-19 disease (AC) and in lung tissue obtained after transplant rejection (TR). (A) unpaired two-tailed t-test, **P<0.01 vs. ctrl, #P<0.05 vs. PGE2, (B, C) One sample t-test, **P<0.01 vs. ctrl, # P<0.05 vs. serum from COVID-19 patients. (E) Statistical analysis was performed using the generalized linear model with Gaussian distribution and weights adjusted according to the number of ROIs per patient, ***P<0.001 vs. ctrl, ###P<0.001 vs AC. (F, G) unpaired two-tailed t-test, **P<0.01 vs. ctrl, *P<0.05 vs. ctrl.

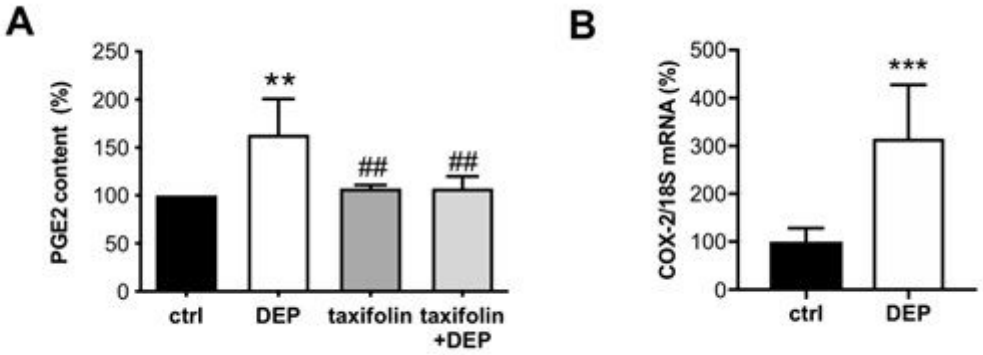

Figure 4

SARS-CoV-2 infection and incubation with Diesel exhaust particles (DEP) are associated with increased expression of COX-2 expression, which is prevented by taxifolin treatment. The bar graph summarizes relative PGE2 levels (in %) of (A) HCEC treated 24h with DEP (10 mg/ml in PBS) (n=12), with taxifolin (100 mm in DMSO) (n=6) or with taxifolin and DEP (n=6) compared with ctrl PBS/DMSO (n=12). The bar graph summarizes COX-2 mRNA levels of (B) HCEC treated 24h with DEP (10 mg/ml in PBS) (n=7) compared with ctrl PBS (n=7). (A+B) Data are presented as mean±SD, the mean of the HCEC ctrl was set at 100 %, (A) **P<0.01, vs. HCEC ctrl PBS, ##P<0.01, vs. HCEC DEP, One sample t-test, (B) ***P<0.001, vs. HCEC ctrl PBS, unpaired two-tailed t-test.

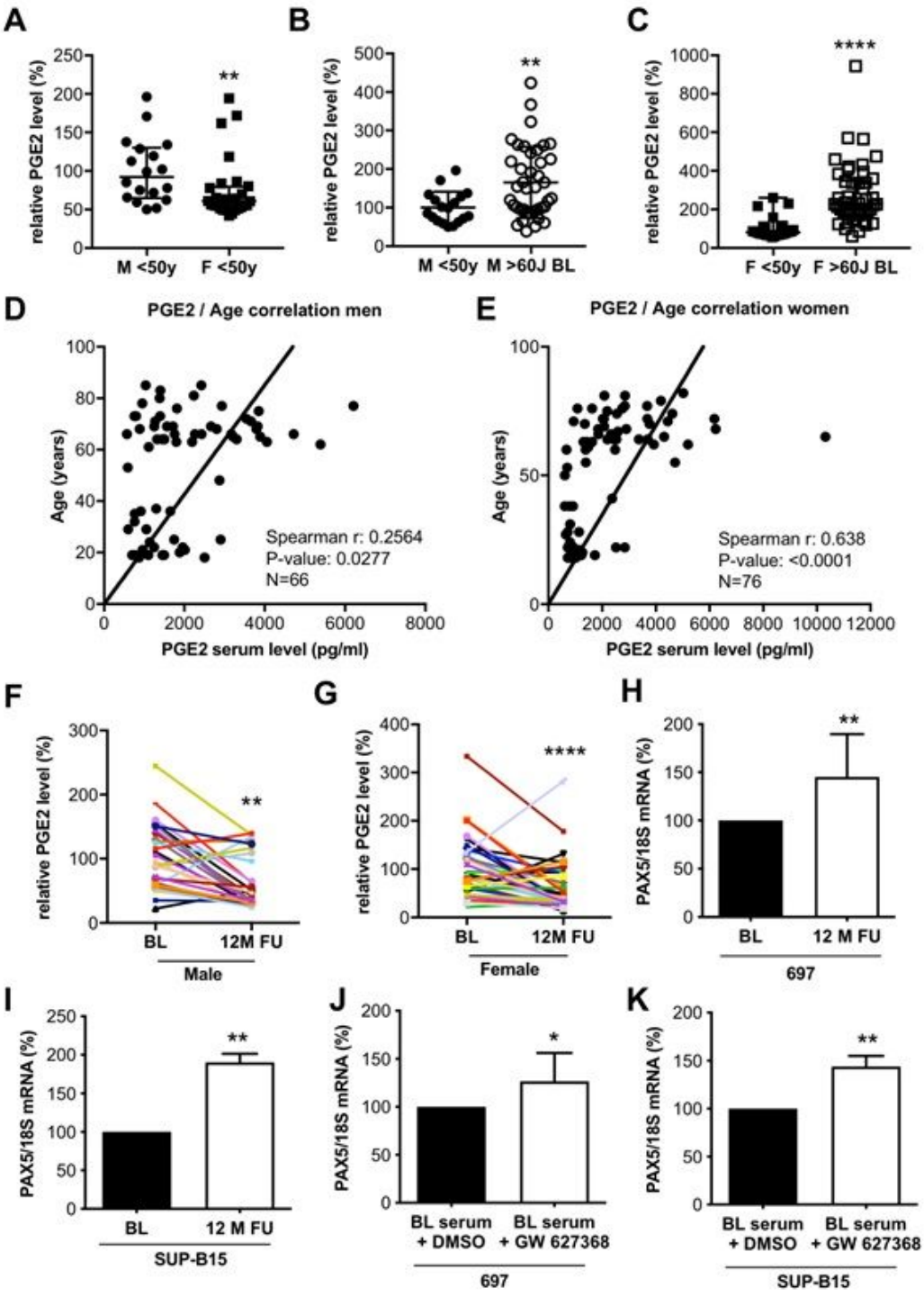

Figure 5

Circulating PGE2 levels in healthy individuals in relation to sex and age. (A) The dot plots summarize relative circulating serum PGE2 levels (in %) of males (n=18) and females (n=28) below the age of 50 years; the median for males was set at 100 %. (B) The dot plots summarize relative circulating serum PGE2 levels (in %) of males (n=18) <50y and males (n=28) >60y; the median for males <50y was set at 100 %. (C) Dot plots summarize relative circulating serum PGE2 levels (in %) of females (n=28) <50y and

females (n=46) >60y, median of females <50y was set at 100 %. Ozone correlation analysis of serum PGE2 levels with age in (D) males (n=66, Spearman r: 0.2564, P-value: 0.0377) and (E) females (n=76, Spearman r: 0.638, P-value: <0.0001). Relative circulating serum PGE2 levels at baseline (BL) and after 12-months follow-up (FU) following controlled physical training from (F) males (n=31) and (G) females (n=39), BL was set at 100%. (H) The bar graph summarizes PAX5 mRNA expression of 697 pre-B-cells treated with human serum collected at BL and after 12-months FU of controlled physical training (n=11). (I) The bar graph summarizes PAX5 mRNA expression of SUP-B15 pre-B-cells treated with human serum collected at BL and after 12-months FU of controlled physical training (n=4). The bar graph summarizes PAX5 mRNA expression of (J) 697 (n=11) and (K) SUP-B15 (n=2) pre-B-cells treated with serum from elderly individuals with high PGE2 levels with and without GW627368 (10 μM). Control pre-B cells were treated with the solvent DMSO. (A, C) Data are presented as median±IQR, **P<0.01, ****P<0.0001, Mann-Whitney-U test. (B) Data are presented as mean±SD, **P<0.01, unpaired two-tailed t-test. (D, E) Ozone correlation, Spearman correlation coefficients, two-tailed P value. (F, G) Data are presented as mean±SD, **P<0.01, ****P<0.0001 unpaired two-tailed t-test. (H, I-J) One sample t-test, **P<0.01 vs. ctrl or BL, **P<0.01 vs. ctrl *P<0.05 vs. ctrl; the mean of ctrl was set at 100 %.

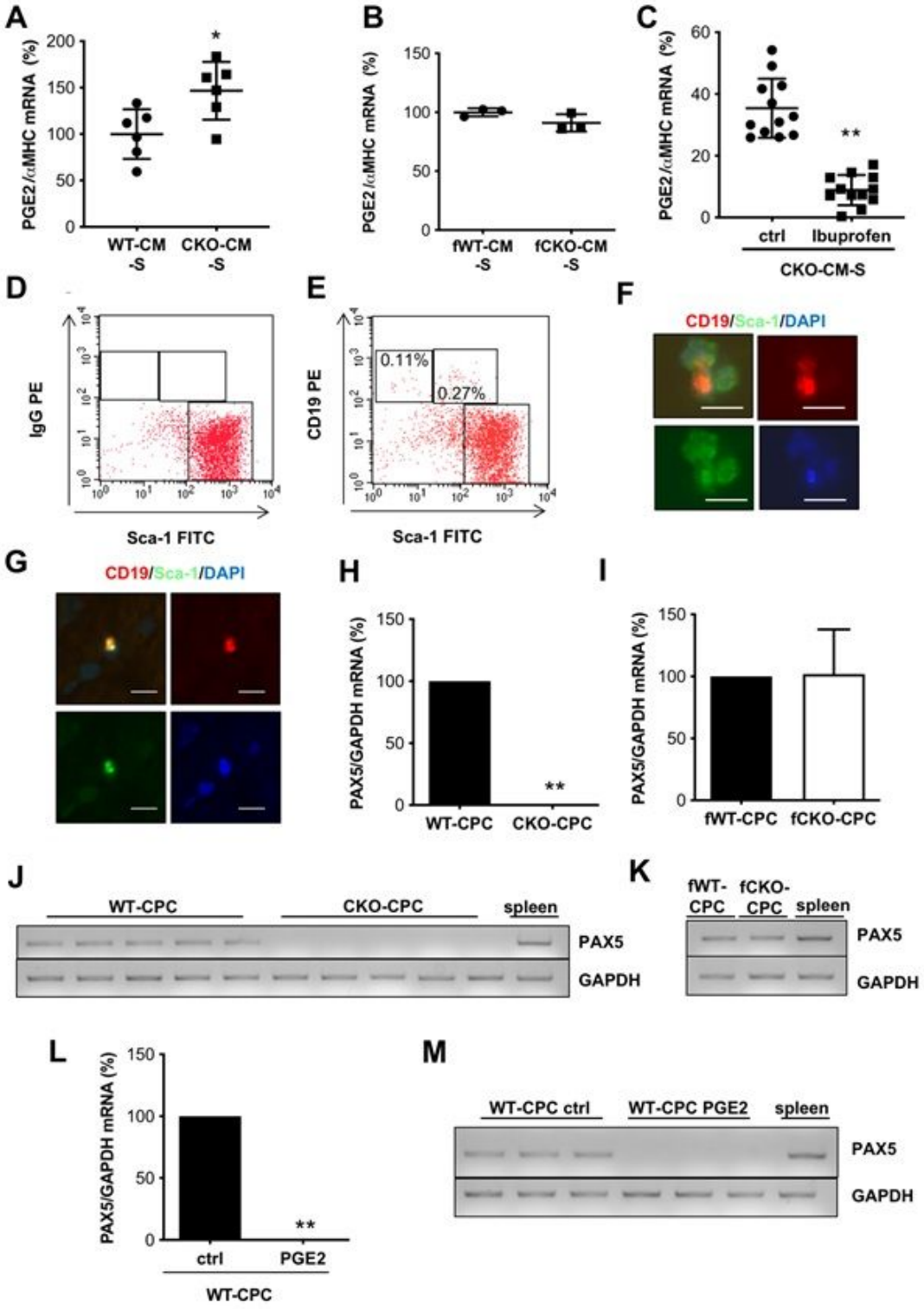

Figure 6

PGE2 levels in cardiomyocytes and PAX5 in CPC isolated from male and female STAT3-CKO mice. The dot plots summarize PGE2 levels in supernatants normalized to aMHC mRNA expression of cardiomyocytes isolated from (A) male, (B) female WT and CKO mice and (C) from CKO mice with and without treatment with ibuprofen, 10 mg/kg bodyweight (cardiomyocytes isolated from (A) and (C) n=6 mice per genotype, (B) n=2-3 mice per genotype). (D, E) FACS analyses showing male WT-CPC after Sca-1

MACS separation stained with Sca-1-FITC and the pre-B-cell marker CD19-PE antibodies ((D) IgG-PE and Sca-1-FITC, (E) CD19-PE and Sca-1-FITC) showing 0.11% Sca-1low/CD19+ and 0.27% Sca-1high/CD19+ cells. Data are pooled from n=15 WT LVs. Acquisition of > 30,000 events was performed. (F) Cytospin of isolated Sca-1-FITC+ CPC co-stained for CD19-PE and DAPI. Scale bar represents 25 µm. (G) Immunofluorescence staining of CD19 (red), Sca-1 (green) and DAPI (blue) in cryosections of heart tissue (WT mice), scale bars: 20 µm. qRT-PCR analysis as bar graphs (H, I) and loaded on gel (I, J) of PAX5 in freshly isolated STAT3-CKO- and WT-CPC from male (H, J, n=5 isolations with each isolation consisting of 8-12 male animals) and from female (I, K, CPC isolated and pooled from 3 WT and 2 CKO mice) WT and STAT3-CKO mice. Bar graph (L) and gel (M) of qRT-PCR analysis of PAX5 in male WT-CPC with and without addition of PGE2 (1 µM) for 48 h. (A, B) mean of WT was set at 100 %, (C) mean of untreated STAT3-CKO was set at 100%, *P<0.05 vs. WT (A, B) or untreated STAT3-CKO (C), unpaired two-tailed t-test (A, B, C). (H, I, L) mean of WT was set at 100 %, **P<0.01 vs. WT (H, I) or ctrl (L), one-sample t-test.

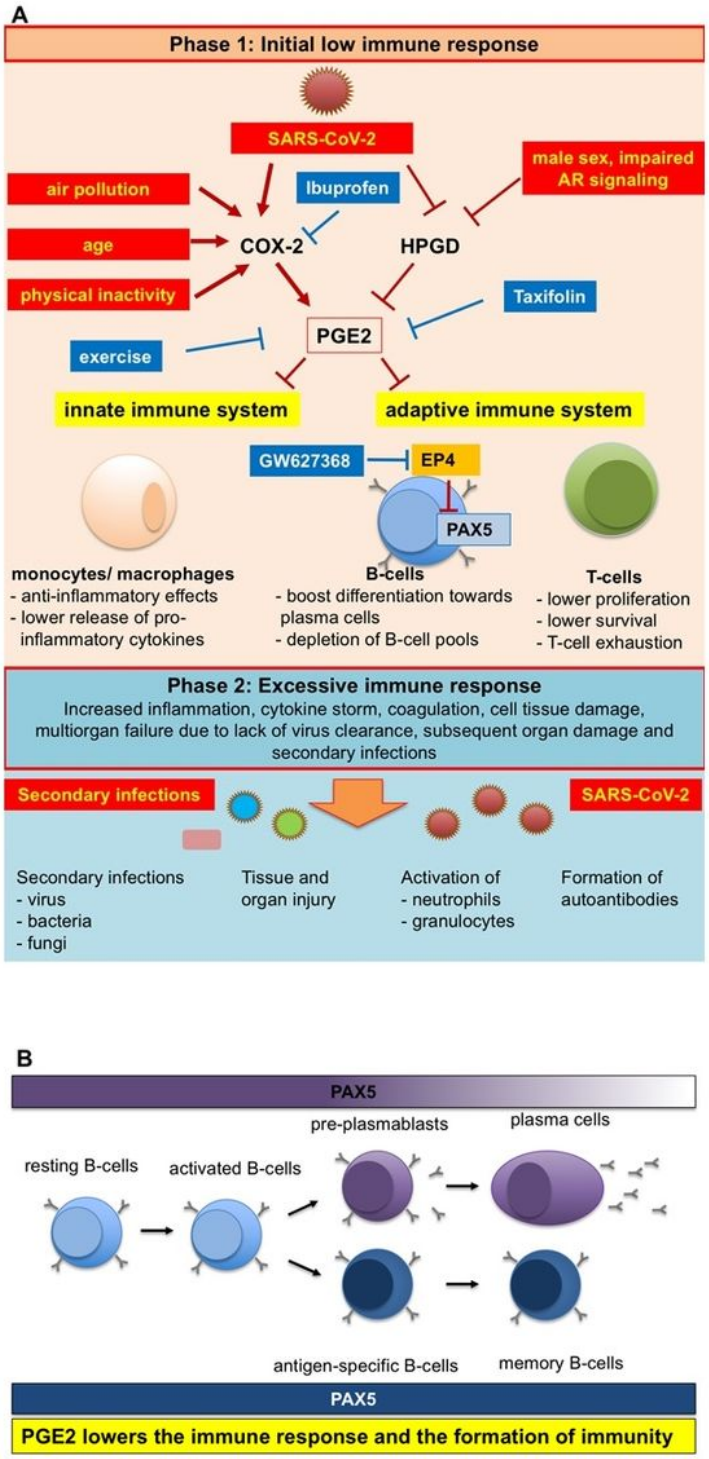

Figure 7

<p>Schematic representation of pleiotropic influences of SARS-CoV-2 infection, air pollution, sex, physical activity and age on PGE2 levels and the ensuing altered immune response. (A) Modulators of PGE2 synthesis and degradation are SARS-CoV-2 infection, but also air pollution, male sex, physical inactivity, and older age, which are all risk factors for more severe COVID-19 disease courses ^{7, 13, 14, 15}. These modulators upregulate the expression of the PGE2-generating enzyme

COX-2 and at least in part reduce the expression of the PGE2-degrading enzyme HPGD, which results in increased generation and secretion of PGE2. PGE2 targets the innate immune system (monocytes/macrophages), where it lowers its efficacy to remove pathogens in part by reducing the release of cytokines ⁵⁴ ⁵⁵. Additionally, PGE2 impairs the response of the adaptive immune system against pathogens by lowering proliferation and survival of T-cells and inducing T-cell ^{2, 37, 38, 53}. Furthermore, PGE2 is impairing the B-cell response to pathogens in part by directly suppressing the B-cell specific transcription factor PAX5 ⁴⁶. Increased PGE2 secretion can be prevented by physical exercise, reduced air pollution and treatment with COX-inhibitors such as ibuprofen or by more specific PGE2 inhibitors such as taxifolin. In addition, taxifolin reduces viral replication. The low immune response (phase 1) may enable the entry of secondary infections with bacteria and fungi and reinfections with SARS-CoV-2 associated with tissue and organ injury, formation of autoantibodies potentially leading to a cytokine storm and an excessive immune response ^{20, 21, 22}[,] ²³[,]²⁴. (B) In pre-B-cells, PAX5 is responsible for suppressing other hematopoietic differentiation programs and promotes proliferation, survival and differentiation of pre-B-cells ^{43, 44, 45} . PGE2 reduces PAX5 expression via its EP4 receptor, which not only reduces their survival and proliferation but boosts the differentiation of B-cells towards plasma cells and may even allow transdifferentiation, features that may lead to the cytokine storm but also the depletion of the B-cell pool (and germinal centers) ¹⁹ ⁴³. In addition, since PAX5 is important for the formation memory cells, PGE2 is therefore also lowering the formation of immunity ^{45, 49}. Blocking the EP4 signaling with the EP4 receptor antagonist GW627368 prevents downregulation of PAX5 in pre-B-cells and may improve viral defense and formation of immunity against SARS-CoV-2.</p>

Supplementary Files

This is a list of supplementary files associated with this preprint. Click to download.

- SupplementaryMaterialsfinal.pdf